

Title	Tissue-specific geometry and chemistry of modern and fossilized melanosomes reveal internal anatomy of extinct vertebrates
Authors	Rossi, Valentina;McNamara, Maria E.;Webb, Sam M.;Ito, Shosuke;Wakamatsu, Kazumasa
Publication date	2019-08-19
Original Citation	Rossi, V., McNamara, M. E., Webb, S. M., Ito, S. and Wakamatsu, K. (2019) 'Tissue-specific geometry and chemistry of modern and fossilized melanosomes reveal internal anatomy of extinct vertebrates', Proceedings of the National Academy of Sciences, 116(36), pp. 17880-17889. DOI: 10.1073/pnas.1820285116
Type of publication	Article (peer-reviewed)
Link to publisher's version	https://www.pnas.org/content/116/36/17880 - 10.1073/pnas.1820285116
Rights	©2019 the Author(s). Published by PNAS. This open access article is distributed under Creative Commons Attribution-NonCommercial-NoDerivatives License 4.0 (CC BY-NC-ND). - https://creativecommons.org/licenses/by-nc-nd/4.0/
Download date	2023-05-04 20:26:58
Item downloaded from	http://hdl.handle.net/10468/8770



UCC

University College Cork, Ireland
 Coláiste na hOllscoile Corcaigh

Tissue-specific geometry and chemistry of modern and fossilized melanosomes reveal internal anatomy of extinct vertebrates

Valentina Rossi^{a,1}, Maria E. McNamara^{a,1}, Sam M. Webb^b, Shosuke Ito^c, and Kazumasa Wakamatsu^c

^aSchool of Biological, Earth and Environmental Sciences, University College Cork, T23 TK30 Cork, Ireland; ^bSLAC National Accelerator Laboratory, Stanford Synchrotron Radiation Lightsource (SSRL), Menlo Park, CA 94025; and ^cDepartment of Chemistry, Fujita Health University School of Health Sciences, 470-1192 Toyoake, Aichi, Japan

Edited by Roy A. Wogelius, University of Manchester, Manchester, United Kingdom, and accepted by Editorial Board Member David Jablonski July 3, 2019 (received for review November 28, 2018)

Recent discoveries of nonintegumentary melanosomes in extant and fossil amphibians offer potential insights into the physiological functions of melanin not directly related to color production, but the phylogenetic distribution and evolutionary history of these internal melanosomes has not been characterized systematically. Here, we present a holistic method to discriminate among melanized tissues by analyzing the anatomical distribution, morphology, and chemistry of melanosomes in various tissues in a phylogenetically broad sample of extant and fossil vertebrates. Our results show that internal melanosomes in all extant vertebrates analyzed have tissue-specific geometries and elemental signatures. Similar distinct populations of preserved melanosomes in phylogenetically diverse vertebrate fossils often map onto specific anatomical features. This approach also reveals the presence of various melanosome-rich internal tissues in fossils, providing a mechanism for the interpretation of the internal anatomy of ancient vertebrates. Collectively, these data indicate that vertebrate melanosomes share fundamental physiological roles in homeostasis via the scavenging and sequestering of metals and suggest that intimate links between melanin and metal metabolism in vertebrates have deep evolutionary origins.

fossil melanin | synchrotron X-ray fluorescence | soft tissue | taphonomy | metallome

Melanins are a family of widely expressed (1) and highly cross-linked (2) pigments derived from the oxidation of the amino acid tyrosine (3). In vertebrates, melanin is packaged as supermolecular aggregates (4) within micrometer-sized organelles termed melanosomes (or melanin granules) (5). Evidence of melanin and melanosomes in diverse fossils (reviewed in refs. 6 and 7) is forging a new paradigm in paleobiology, allowing inferences of the adaptive coloration and behavior of extinct taxa (8, 9) (although these interpretations are not without limitations) (5–7). In addition to studies of coloration *sensu stricto* [e.g., of melanin-based patterning (10), structural coloration, and melanosome diversity (9, 11, 12) in fossil feathers and of countershading in ancient vertebrates (8, 13–17)], recent studies have highlighted the chemical taphonomy of melanin (2, 15, 18, 19), the melanin metallome (20, 21), and the evolution of integumentary melanosomes (22). Recent evidence for nonintegumentary melanin (extracutaneous) (5) (i.e., from internal tissues, excluding the eyes) in extant vertebrates and fossil amphibians (23, 24) supports hypotheses that melanosomes may have broader functions beyond integumentary coloration (25). Internal melanin is implicated in protection against pollutants, free radicals, low temperatures, and in organ development and function (reviewed in ref. 23). Excepting a single study on amphibians (24), however, previous paleontological studies have considered primarily integumentary and ocular melanosomes, revealing aspects of their geometry (11, 22, 26, 27), chemistry (2, 19, 28, 29), and metal content (20, 30, 31). The phylogenetic distribution and evolutionary history of internal melanosomes, however, have not been evaluated systematically.

This is essential to accurate interpretations of fossil melanosomes and for understanding the functional evolution of melanin through deep time.

Here, we report the anatomical distribution, abundance, geometry, melanin chemistry, and elemental inventory of melanosomes in tissues from 15 extant vertebrate taxa, coupled with data on the distribution, geometry, and chemistry of preserved melanosomes in fossils (Table 1). We extracted melanosomes from 243 tissue samples of extant vertebrates ([Dataset S1](#) and [SI Appendix](#)) using a modified enzymatic melanosome extraction (EME) process (26) and sampled melanosome-rich soft tissues in fossils ([Dataset S2](#)). Melanin chemistry was analyzed for selected samples ([Dataset S1](#)) using alkaline hydrogen peroxide oxidation (AHPO) (4), a chemical assay used to quantify the concentration of melanin-specific molecular markers present in modern (32) and fossil (2) samples. The AHPO results are supported by Warthin–Starry staining of histological sections ([Dataset S1](#)), which produces diagnostic results for melanin (33) ([SI Appendix](#)). Scanning electron microscopy (SEM) and synchrotron rapid scanning X-ray fluorescence (SRS-XRF) were used to analyze the geometry and major-to-trace elemental chemistry, respectively, of extracted and fossil melanosomes (including, for SRS-XRF, analysis of whole untreated fossil specimens) ([Dataset S2](#)). For SRS-XRF, we analyzed the concentrations of 11 elements: phosphorous (P), sulfur (S), chlorine (Cl), potassium (K), calcium

Significance

Recent reports of nonintegumentary melanosomes in fossils hint at functions for melanin beyond color production, but the biology and evolution of internal melanosomes are poorly understood. Our results show that internal melanosomes are widespread in diverse fossil and modern vertebrates and have tissue-specific geometries and metal chemistries. Tissue-specific chemical signatures can persist in fossils despite some diagenetic overprint, allowing the reconstruction of internal soft-tissue anatomy in fossil vertebrates, and suggest that links between melanin and metal regulation have deep evolutionary origins in vertebrates.

Author contributions: V.R. and M.E.M. designed research; V.R., M.E.M., S.I., and K.W. performed research; S.M.W., S.I., and K.W. contributed new reagents/analytic tools; V.R., S.I., and K.W. analyzed data; and V.R. and M.E.M. wrote the paper.

The authors declare no conflict of interest.

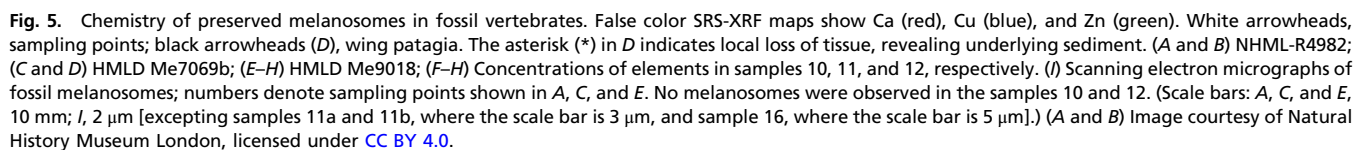
This article is a PNAS Direct Submission. R.A.W. is a guest editor invited by the Editorial Board.

This open access article is distributed under [Creative Commons Attribution-NonCommercial-NoDerivatives License 4.0 \(CC BY-NC-ND\)](#).

¹To whom correspondence may be addressed. Email: valentina.rossi@ucc.ie or maria.mcnamara@ucc.ie.

This article contains supporting information online at www.pnas.org/lookup/suppl/doi:10.1073/pnas.1820285116/-DCSupplemental.

Published online August 19, 2019.



PNAS | September 3, 2019 | vol. 116 | no. 36 | 17885

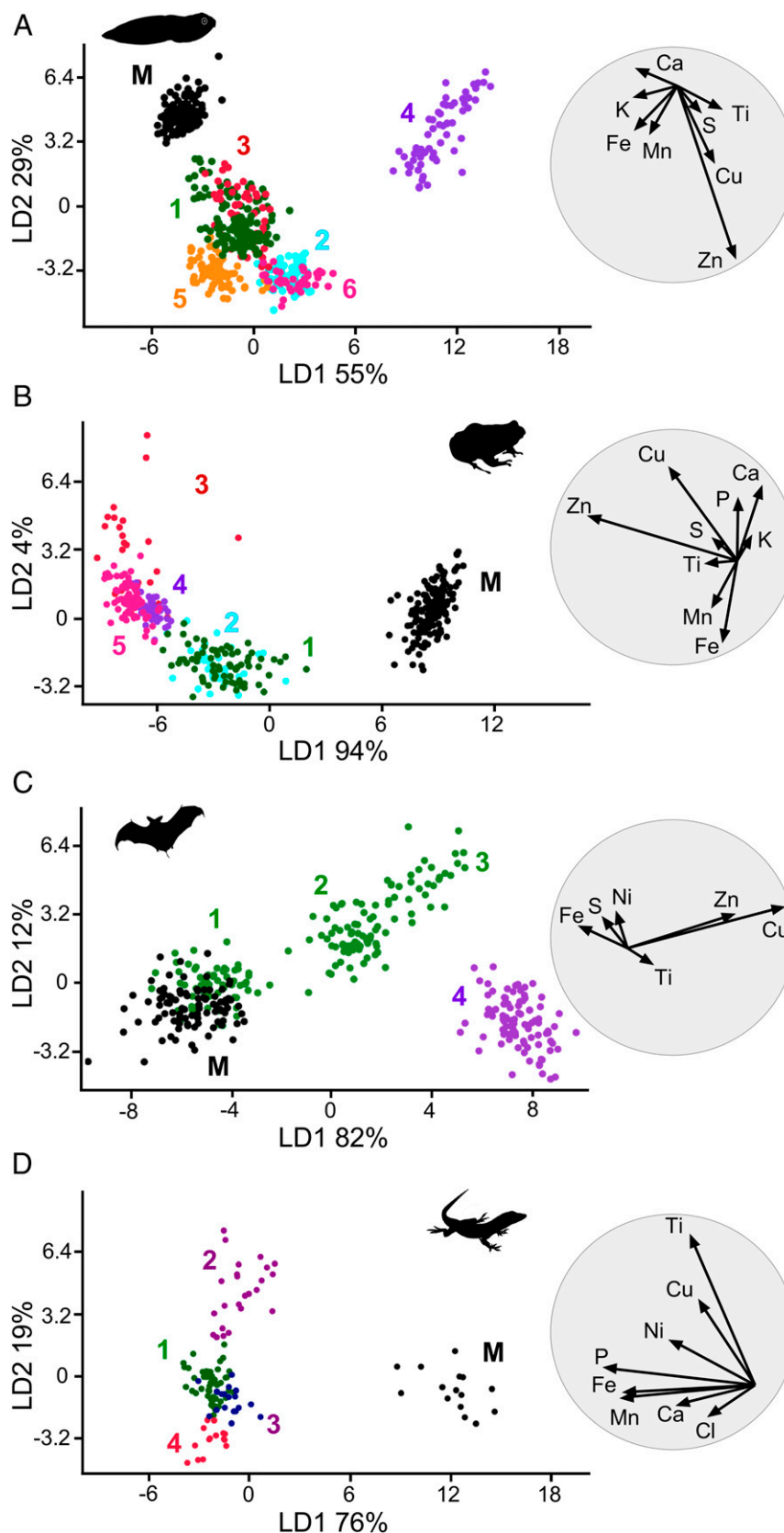


Fig. 6. Linear discriminant analysis of elemental chemistry of fossil melanosomes. (A) NHML-R4999 (*P. pueyoi*, Libros). (B) NHML-R4982 (*P. pueyoi*, Libros). (C) HMLD Me7069b (Chiroptera indet., Messel). (D) HMLD Me9018 (Reptilia indet., Messel). Each LDA plot is accompanied by a biplot (to the right). Numbers denote regions of interest (ROIs) (*SI Appendix*, Fig. S22) mapped using SRS-XRF; note that these numbers do not correspond to the sampling points for SEM analysis. M denotes sedimentary matrix (A–C) or resin (D). Colors that correspond to unequivocal organs: green, skin; cyan, eyespot; magenta, other soft tissue features.

tissue samples were used for melanin extraction ($n = 243$) and SRS-XRF ($n = 183$) than for AHPO ($n = 32$) or histology ($n = 28$). *Troglodytes troglodytes* tissues were available only for AHPO analysis.

Fossil Specimens. Specimens were selected where soft tissues were preserved as a dark-colored, near-2D film. Specimens were from different depositional and diagenetic environments (Dataset S2). Institutional abbreviations are as follows: Hessisches Landesmuseum Darmstadt (HLMD) and Natural History Museum London (NHML).

Enzymatic Melanin Extraction. A total of 243 tissues samples were selected for study (3 replicates of each of 81 tissues). Tissues were dissected with sterile tools and processed immediately or stored at -80°C before EME. Melanin was extracted using a modified version of the protocol in ref. 26. In brief, samples were treated with 9 cycles of solutions using 1,4-DTT (DTT), proteinase-K, and papain while incubated at 37.5°C at 200 rpm for 9 d (SI Appendix).

Alkaline Hydrogen Peroxide Oxidation. Alkaline hydrogen peroxide oxidation is a unique chemical assay for melanin that produces diagnostic chemical markers (e.g., pyrrole-2,3,5-tricarboxylic acid [PTCA], pyrrole-2,3-dicarboxylic acid [PDCA], and pyrrole-2,3,4,5-tetracarboxylic acid [PTeCA], which are derived from the dihydroxyindole parent subunit of the melanin molecule) that allow identification and quantification of melanin in modern and fossil materials (2, 4). Freeze-dried samples ($n = 32$) of skin, heart, liver, lungs, connective tissue, spleen, kidney, and hair of extant taxa (9 to 17 mg) were homogenized in water with a Ten-Broeck homogenizer at a concentration of 10 mg/mL. Aliquots (200 μL) were dried in a desiccator and subjected to acid hydrolysis with 6 M HCl (0.5 mL) at 110°C for 16 h (32). This acid hydrolysis removes proteins and small molecules that might interfere with the assay and thus increases specificity of the biomarkers (32). The resulting insoluble materials including melanin were collected by centrifugation and washed once with water as described previously (32). The residues were then subjected to alkaline hydrogen peroxide oxidation (AHPO) (4). Aliquots (100 μL) of tissue suspensions were also subjected to hydroiodic acid hydrolysis to analyze 4-amino-3-hydroxyphenylalanine (4-AHP), a specific biomarker for pheomelanin (34). A sample of soft tissues from a fossil frog from the Late Miocene Libros biota (MNCN 63776) was finely ground with a mortar and pestle and weighed. The powder was subjected to acid hydrolysis and AHPO analysis as above (4).

Histology. Tissues were dissected using sterile tools ($n = 28$), fixed with 75% ethanol, and embedded in paraffin wax. Histological sections (9 μm thick) were stained with the Warthin–Starry stain for melanin, which is considered more specific and sensitive to melanin than other histological stains (33) (SI Appendix). The percentage area of tissue occupied by melanin was calculated for each section by analyzing digital photographs using the Threshold

Color plugin in ImageJ (54). Values cited here are mean values calculated from three representative images for each tissue. The values of the SDs are higher than the mean values; this is likely to happen when working with a small dataset showing a vast range of values.

Scanning Electron Microscopy. Fossil samples and melanin extracts were placed on aluminum stubs, coated with Au/Pd, and examined using an FEI Inspect F FE-SEM at an accelerating voltage of 5 to 10 kV. Extracts were screened using SEM, and only extracts containing pristine melanosomes ($n = 95$) (SI Appendix, Figs. S2–S4 and Dataset S1) were analyzed further. For each fossil sample and melanin extract, long and short axes of 50 melanosomes orientated perpendicular to line of sight were measured in ImageJ. Data were analyzed using R (55) and PAST (56).

Synchrotron Rapid-Scanning X-Ray Fluorescence. Rapid-scanning synchrotron-based X-ray fluorescence data were collected at the Stanford Synchrotron Radiation Lightsources using beam line 10-2. The incident X-ray energy was set to 11 keV using an Si (111) double crystal monochromator with the storage ring containing 500 mA in top-off mode at 3.0 GeV. A microfocused beam of $2 \times 2 \mu\text{m}$ was provided by an Rh-coated Kirkpatrick–Baez mirror pair, pixel size $25 \times 25 \mu\text{m}$. The incident X-ray intensity was measured with a nitrogen-filled ion chamber. Specimens were mounted at 45° to the incident X-ray beam and were spatially rastered at 50 ms per pixel dwell time. The entire fluorescence spectrum was collected at each data point, and the intensity of fluorescence lines for selected elements (P, S, Cl, K, Ca, Ti, Mn, Fe, Ni, Cu, and Zn) was monitored using a silicon drift Vortex detector. Fluorescence intensities were corrected for detector deadtime and distance to allow comparison among samples. The concentrations of each element in $\mu\text{g}/\text{cm}^2$ were calibrated using NIST traceable thin film elemental standards. Data processing was performed using MicroAnalysis Toolkit software (57) (SI Appendix). Regions of interest for quantitative analysis were selected for each specimen. For each region of interest, raw pixel data, mean and SD values were calculated for the concentrations of each element. Differences in elemental concentrations between regions of interest were assessed using Linear Discriminant Analysis (LDA) in PAST. See SI Appendix for further details of SRS-XRF methods.

ACKNOWLEDGMENTS. We thank Roy Wogelius and 3 anonymous reviewers for their thoughtful and constructive comments. We thank Courtney Roach, Nick Edwards, Enrico Pirota, Sharon Lynch, Babette Brooklar, Nick Hou, Chris Rogers, Naomi O'Reilly, Giliane Odin, Joe Tobin, Luke Harman, Carmel Hensey, Vince Lodge, Patricia Vernon, John Bainbridge, Liam Hayes, and Twomey's Butchers Macrooom for assistance. This work was funded by European Research Council Starting Grant ERC-2014-StG-637691-ANICOLEVO (to M.E.M.). Use of the Stanford Synchrotron Radiation Lightsources, SLAC National Accelerator Laboratory, is supported by the US Department of Energy, Office of Science, Office of Basic Energy Sciences under Contract DE-AC02-76SF00515.

1. I. Galván, F. Solano, Melanin chemistry and the ecology of stress. *Physiol. Biochem. Zool.* **88**, 352–355 (2015).
2. K. Glass et al., Direct chemical evidence for eumelanin pigment from the Jurassic period. *Proc. Natl. Acad. Sci. U.S.A.* **109**, 10218–10223 (2012).
3. P. A. Riley, Melanin. *Int. J. Biochem. Cell Biol.* **29**, 1235–1239 (1997).
4. S. Ito et al., Usefulness of alkaline hydrogen peroxide oxidation to analyze eumelanin and pheomelanin in various tissue samples: Application to chemical analysis of human hair melanins. *Pigment Cell Melanoma Res.* **24**, 605–613 (2011).
5. J. J. Negro, C. Finlayson, I. Galván, Melanins in fossil animals: Is it possible to infer life history traits from the coloration of extinct species? *Int. J. Mol. Sci.* **19**, E230 (2018).
6. J. Lindgren et al., Interpreting melanin-based coloration through deep time: A critical review. *Proc. Biol. Sci.* **282**, 20150614 (2015).
7. N. P. Edwards, P. L. Manning, R. A. Wogelius, Pigments through time. *Pigment Cell Melanoma Res.* **27**, 684–685 (2014).
8. J. Vinther et al., 3D camouflage in an ornithischian dinosaur. *Curr. Biol.* **26**, 2456–2462 (2016).
9. D. Hu et al., A bony-crested Jurassic dinosaur with evidence of iridescent plumage highlights complexity in early paravian evolution. *Nat. Commun.* **9**, 217 (2018).
10. Q. Li et al., Plumage color patterns of an extinct dinosaur. *Science* **327**, 1369–1372 (2010).
11. Q. Li et al., Reconstruction of *Microraptor* and the evolution of iridescent plumage. *Science* **335**, 1215–1219 (2012).
12. J. A. Clarke et al., Fossil evidence for evolution of the shape and color of penguin feathers. *Science* **330**, 954–957 (2010).
13. C. M. Brown et al., An exceptionally preserved three-dimensional armored dinosaur reveals insights into coloration and cretaceous predator-prey dynamics. *Curr. Biol.* **27**, 2514–2521.e3 (2017).
14. F. M. Smithwick, R. Nicholls, I. C. Cuthill, J. Vinther, Countershading and stripes in the theropod dinosaur *Sinosauropteryx* reveal heterogeneous habitats in the early cretaceous Jehol biota. *Curr. Biol.* **27**, 3337–3343.e2 (2017).
15. M. E. McNamara et al., Reconstructing carotenoid-based and structural coloration in fossil skin. *Curr. Biol.* **26**, 1075–1082 (2016).
16. S. E. Gabbott et al., Pigmented anatomy in Carboniferous cyclostomes and the evolution of the vertebrate eye. *Proc. Biol. Sci.* **283**, 20161151 (2016).
17. J. Lindgren et al., Skin pigmentation provides evidence of convergent melanism in extinct marine reptiles. *Nature* **506**, 484–488 (2014).
18. J. Lindgren et al., Biochemistry and adaptive colouration of an exceptionally preserved juvenile fossil sea turtle. *Sci. Rep.* **7**, 13324 (2017).
19. C. Colleary et al., Chemical, experimental, and morphological evidence for diagenetically altered melanin in exceptionally preserved fossils. *Proc. Natl. Acad. Sci. U.S.A.* **112**, 12592–12597 (2015).
20. R. A. Wogelius et al., Trace metals as biomarkers for eumelanin pigment in the fossil record. *Science* **333**, 1622–1626 (2011).
21. N. P. Edwards et al., Elemental characterisation of melanin in feathers via synchrotron X-ray imaging and absorption spectroscopy. *Sci. Rep.* **6**, 34002 (2016).
22. Q. Li et al., Melanosome evolution indicates a key physiological shift within feathered dinosaurs. *Nature* **507**, 350–353 (2014).
23. S. Dubey, A. Roulin, Evolutionary and biomedical consequences of internal melanins. *Pigment Cell Melanoma Res.* **27**, 327–338 (2014).
24. M. E. McNamara et al., Non-integumentary melanosomes can bias reconstructions of the colours of fossil vertebrates. *Nat. Commun.* **9**, 2878 (2018).
25. J. Vinther, A guide to the field of palaeo colour: Melanin and other pigments can fossilise: Reconstructing colour patterns from ancient organisms can give new insights to ecology and behaviour. *Bioessays* **37**, 643–656 (2015).

26. Y. Liu *et al.*, Comparison of the structural and physical properties of human hair eumelanin following enzymatic or acid/base extraction. *Pigment Cell Res.* **16**, 355–365 (2003).
27. Y. Pan *et al.*, Molecular evidence of keratin and melanosomes in feathers of the Early Cretaceous bird *Eoconfuciusornis*. *Proc. Natl. Acad. Sci. U.S.A.* **113**, E7900–E7907 (2016).
28. J. Lindgren *et al.*, Molecular preservation of the pigment melanin in fossil melanosomes. *Nat. Commun.* **3**, 824 (2012).
29. T. Clements *et al.*, The eyes of *Tullimonstrum* reveal a vertebrate affinity. *Nature* **532**, 500–503 (2016).
30. N. P. Edwards *et al.*, Infrared mapping resolves soft tissue preservation in 50 million year-old reptile skin. *Proc. Biol. Sci.* **278**, 3209–3218 (2011).
31. V. M. Egerton *et al.*, The mapping and differentiation of biological and environmental elemental signatures in the fossil remains of a 50 million year old bird. *J. Anal. At. Spectrom.* **30**, 627–634 (2015).
32. S. Ito *et al.*, Acid hydrolysis reveals a low but constant level of pheomelanin in human black to brown hair. *Pigment Cell Melanoma Res.* **31**, 393–403 (2018).
33. N. Joly-Tonetti, J. I. D. Wibawa, M. Bell, D. Tobin, Melanin fate in the human epidermis: A reassessment of how best to detect and analyse histologically. *Exp. Dermatol.* **25**, 501–504 (2016).
34. K. Wakamatsu, S. Ito, J. L. Rees, The usefulness of 4-amino-3-hydroxyphenylalanine as a specific marker of pheomelanin. *Pigment Cell Res.* **15**, 225–232 (2002).
35. C. M. Eliason, J. A. Clarke, Metabolic physiology explains macroevolutionary trends in the melanic colour system across amniotes. *Proc. Biol. Sci.* **285**, 20182014 (2018).
36. C. D. Faraco, S. A. Vaz, M. V. Pástor, C. A. Erickson, Hyperpigmentation in the Silkie fowl correlates with abnormal migration of fate-restricted melanoblasts and loss of environmental barrier molecules. *Dev. Dyn.* **220**, 212–225 (2001).
37. J. K. Hubbard, J. A. C. Uy, M. E. Hauber, H. E. Hoekstra, R. J. Safran, Vertebrate pigmentation: From underlying genes to adaptive function. *Trends Genet.* **26**, 231–239 (2010).
38. Y. X. C. Bourgeois *et al.*, A novel locus on chromosome 1 underlies the evolution of a melanic plumage polymorphism in a wild songbird. *R. Soc. Open Sci.* **4**, 160805 (2017).
39. A. Roulin, Melanin-based colour polymorphism responding to climate change. *Glob. Change Biol.* **20**, 3344–3350 (2014).
40. I. Galván, A. P. Møller, J. Erritzoe, Testicular melanization has evolved in birds with high mtDNA mutation rates. *J. Evol. Biol.* **24**, 988–998 (2011).
41. F. Solano, Melanins: Skin pigments and much more—types, structural models, biological functions, and formation routes. *New J. Sci.* **2014**, 1–28 (2014).
42. J. M. Wood *et al.*, What's the use of generating melanin? *Exp. Dermatol.* **8**, 153–164 (1999).
43. A. Jakimska, P. Konieczka, K. Skóra, J. Namieśnik, Bioaccumulation of metals in tissues of marine animals, part I: The role and impact of heavy metals on organism. *Pol. J. Environ. Stud.* **20**, 1127–1146 (2011).
44. C. Andreini, I. Bertini, G. Cavallaro, G. L. Holliday, J. M. Thornton, Metal ions in biological catalysis: From enzyme databases to general principles. *J. Biol. Inorg. Chem.* **13**, 1205–1218 (2008).
45. M. L. Bender, Metal ion catalysis of nucleophilic organic reactions in solution. *Adv. Chem. Ser.* **37**, 19–36 (1962).
46. M. Kleczkowski, M. Garncarz, The role of metal ions in biological oxidation—The past and the present. *Pol. J. Vet. Sci.* **15**, 165–173 (2012).
47. R. W. McDiarmid, R. Altig, *Tadpoles: The Biology of Anuran Larvae* (University of Chicago Press, Chicago, 1999), 458 pp.
48. D. W. Choi *et al.*, Spectral and thermodynamic properties of Ag(I), Au(III), Cd(II), Co(II), Fe(III), Hg(II), Mn(II), Ni(II), Pb(II), U(IV), and Zn(II) binding by methanobactin from *Methylosinus trichosporium* OB3b. *J. Inorg. Biochem.* **100**, 2150–2161 (2006).
49. L. Hong, J. D. Simon, Current understanding of the binding sites, capacity, affinity, and biological significance of metals in melanin. *J. Phys. Chem. B* **111**, 7938–7947 (2007).
50. J. M. Gallas, K. C. Littrell, S. Seifert, G. W. Zajac, P. Thiyagarajan, Solution structure of copper ion-induced molecular aggregates of tyrosine melanin. *Biophys. J.* **77**, 1135–1142 (1999).
51. M. E. McNamara, B. E. van Dongen, N. P. Lockyer, I. D. Bull, P. J. Orr, Fossilization of melanosomes via sulfurization. *Palaeontology* **59**, 337–350 (2016).
52. H. E. Barden *et al.*, Morphological and geochemical evidence of eumelanin preservation in the feathers of the Early Cretaceous bird, *Gansus yumenensis*. *PLoS One* **6**, e25494 (2011).
53. P. L. Manning *et al.*, Synchrotron-based chemical imaging reveals plumage patterns in a 150 million year old early bird. *J. Anal. At. Spectrom.* **28**, 1024 (2013).
54. C. A. Schneider, W. S. Rasband, K. W. Eliceiri, NIH Image to ImageJ: 25 years of image analysis. *Nat. Methods* **9**, 671–675 (2012).
55. R Core Team, R: A Language and Environment for Statistical Computing (Version 1.0.143). <http://www.r-project.org/>. Accessed 1 April 2016.
56. Ø. Hammer, D. A. T. Harper, P. D. Ryan, Paleontological Statistics Software: Package for Education and Data Analysis. 9 (Version 3.12, Øyvind Hammer, Natural History Museum, University of Oslo, Oslo, Norway, 2001).
57. S. M. Webb, The microAnalysis toolkit: X-ray fluorescence image processing software. *AIP Conf. Proc.* **1365**, 196–199 (2010).